



Research article

Sustainable utilization of *Sedum plumbizincicola* as superior hydrochar for efficient nutrients recoveryRuichi Zhang^a, Yizhong Zhang^b, Ronn Goei^c, Wen-Da Oh^d, Zhao Zhang^e, Chao He^{a,*}^a Faculty of Engineering and Natural Sciences, Tampere University, Korkeakoulunkatu 8, 33720, Tampere, Finland^b Seawater Hydrogen Energy and Water Treatment Laboratory, Department of Environmental Technology, The Institute of Seawater Desalination and Multipurpose Utilization, Ministry of Natural Resources (MNR), Tianjin, 300192, China^c School of Materials Science and Engineering, Nanyang Technological University, 50 Nanyang Avenue, Singapore, 639798, Singapore^d School of Chemical Sciences, Universiti Sains Malaysia, 11800, Penang, Malaysia^e Administration Committee of Yancheng Economic and Technological Development Zone, Yancheng, 224000, China

ARTICLE INFO

Keywords:

Hyperaccumulator

Hydrothermal carbonization

Surface functional group

Chemisorption

Synergistic co-adsorption

ABSTRACT

To realize sound disposal of hyperaccumulator harvested from phytoremediation, hydrothermal carbonization (HTC) has been employed to obtain superior hydrochar adsorbents for removal of phosphate and ammonium from water body. A series of hydrochars have been prepared under tuned HTC conditions to tailor hydrochar with desired properties. Generally, increased temperature and prolonged reaction time facilitated acidic oxygen functional groups on hydrochars, thereby improving adsorption capacity of hydrochar. In single solute system, a superior hydrochar, derived from HTC under 260 °C for 2 h, achieved a maximum phosphate and ammonium adsorption capacity of 52.46 mg/g and 27.56 mg/g at 45 °C, respectively. In binary system, synergistic adsorption was observed only in lower solute concentration, whereas competitive adsorption occurred under higher solute concentration. Characterization and adsorption kinetics suggested chemisorption may dominate the adsorption process, thus the adsorption capacity could be improved by tuning pH_{pzc} of hydrochar. This study firstly demonstrates the sustainable utilization of hyperaccumulators into nutrients-enriched hydrochar as fertilizer for *in-situ* phytoremediation of contaminated sites with minimized environmental risks towards circular economy.

1. Introduction

Phytoremediation, known as a green remediation technique, refers to using plants to partially or substantially remediate selected contaminants in soil, sludge, sediment or water (Pivetz, 2001). Owing to its effectiveness, low cost and good acceptance by the general public, phytoremediation of soils contaminated by heavy metals has attracted increasing attention and been well investigated in recent years (Li et al., 2014). For example, *Pteris vittata* was applied to remove 7.8% of total As in soil after seven-month growth (Liao et al., 2004), while 28% of total Cd in the soil was removed by *Sedum alfredii* after a three-year field application (Zhou et al., 2014). Particularly, *Sedum plumbizincicola* (*S. plumbizincicola*) demonstrated a remarkable capability to extract Zn and Cd from Zn/Cd polluted soils (Ma et al., 2013). Nevertheless, after harvesting from phytoremediation sites, sound and safe disposal of hyperaccumulators is essential to avoid secondary pollution.

At present, thermal treatment of metal-enriched hyperaccumulators is considered as an effective technique because of its high conversion efficiency and great volume reduction effect (Cui et al., 2021). However, prior drying of harvested hyperaccumulators with high moisture content is necessary for downstream conventional thermochemical processing. Different from conventional thermal treatment, hydrothermal conversion (i.e., hydrothermal carbonization (HTC), hydrothermal liquefaction (HTL) and hydrothermal gasification (HTG)) could be advantageous for direct disposal of freshly harvested metal-enriched hyperaccumulators with certain moisture content (Cui et al., 2022). Especially, HTC could convert organic materials into hydrochar that can be used as fuel, soil conditioner, adsorbent, and catalyst support (Masoumi et al., 2021). Most of the heavy metals could be immobilized in hydrochar after HTC (Jin et al., 2019; Masoumi et al., 2021). Meanwhile, due to abundant oxygenated functional groups and active sites formed resulting from naturally bonded heavy metals, hydrochar emerged as carbonaceous

* Corresponding author.

E-mail address: chao.he@tuni.fi (C. He).<https://doi.org/10.1016/j.jenvman.2023.118441>

Received 12 March 2023; Received in revised form 29 May 2023; Accepted 15 June 2023

Available online 26 June 2023

0301-4797/© 2023 The Author(s). Published by Elsevier Ltd. This is an open access article under the CC BY license (<http://creativecommons.org/licenses/by/4.0/>).

adsorbent for various pollutants in aquatic environment.

As a consequence of rapid urbanization and industrialization in recent decades, excessive nitrogen (N) and phosphorus (P) have been discharged into water bodies, leading to serious eutrophication. N in water usually exists in different forms, including ammonia-nitrogen ($\text{NH}_3\text{-N}$), nitrate ($\text{NO}_3\text{-N}$), nitrite ($\text{NO}_2\text{-N}$), and organic nitrogen (Al-Ghouti et al., 2019). $\text{NH}_3\text{-N}$ is considered as one of the most severe issues in water pollution control because it could be toxic to aquatic creatures even in a small amount (Francis-Floyd et al., 2009). $\text{NH}_3\text{-N}$ could be transformed into less harmful ammonium-nitrogen (NH_4^+) by adjusting pH, temperature and ionic strength. In most cases, NH_4^+ ($\text{pK}_a = 9.25$ at 25°C) is the dominant species in natural water (Zhang et al., 2020). Besides, the drastically increasing discharge of phosphate accelerated eutrophication (Vikrant et al., 2018). P can exist in both inorganic and organic species in aqueous solution. Orthophosphate (phosphate with only P-O bond) is the dominant inorganic species detected in water, while other species, such as pyrophosphate, hypophosphite, phosphite, etc., are much less (Francis-Floyd et al., 2009). Functional biochar materials have recently been intensively explored as adsorbent for N and P removal from water owing to their large surface area, porosity, stable carbon matrix and easy production (Tan et al., 2017). Recently, hydrochar attracts great attention because of their abundant surface functional groups and lower energy consumption in production as compared to biochar obtained via pyrolysis under higher temperature. Moreover, there is limited research on the application of hydrochar for simultaneous adsorption of N and P.

Therefore, this study aims to remove phosphate and ammonium from aqueous solution using hydrochar derived from *S. plumbizincicola* using HTC. Specific objectives of this research are to 1) screen hydrochar with desired adsorption properties by tuning temperature and reaction time in HTC of *S. plumbizincicola*, and 2) identify the synergistic or competitive adsorption of phosphate and ammonium in a binary system. Thus, comprehensive characterization and analysis of different hydrochar adsorbents will be carried out to understand the effect of various HTC conditions on physicochemical properties of hydrochars. Subsequently, adsorption behaviors of phosphate and ammonium in both single solute and binary systems will be examined to elucidate the mechanism in order to achieve synergy in a binary adsorption system. Given the notion of circular economy, this N and P enriched hydrochar composite will be eventually applied as fertilizer for phytoremediation of contaminated sites to realize sustainable *in-situ* management of hyperaccumulators and minimize any potential environmental risks of secondary pollution.

2. Materials and methods

2.1. Materials

S. plumbizincicola was collected from a Zn contaminated site in Guangdong Province, China, which was washed to remove impurities and dried at 85°C in oven. Dry *S. plumbizincicola* was subsequently ground into fine powders less than 0.5 mm and kept in a desiccator before use. Table 1 presents the physicochemical properties of *S. plumbizincicola*. Specifically, concentration of major metals (e.g., Zn, Fe, and Cd) in the *S. plumbizincicola* was 35,165.50, 7814.71, and

1222.63 mg/kg, respectively. The Zn content (3.52%) in this *S. plumbizincicola* was significantly higher than those common hyper-accumulators ($\sim 0.3\%$ Zn content). Other metal and metalloid trace elements were Pb, Mn, Cr, and As with concentration of 371.54, 313.63, 134.19, and 13.87 mg/kg, respectively. Potassium dihydrogen phosphate and ammonium chloride were purchased from Aladdin. Ascorbic acid was obtained from Macklin. Potassium antimony tartrate, ammonium molybdate, sodium hydroxide and hydrochloric acid were purchased from Guangzhou Chemical Reagent Factory. All the chemicals used in this study were of analytical grade.

2.2. Hyperaccumulator hydrochar preparation

HTC of *S. plumbizincicola* was performed in a 250 mL autoclave (material: Hastelloy C276, model: HT-250JOC, HTLAB, Shanghai HuoTong Experimental Instrument Co., Ltd.). Briefly, 4 g of dried *S. plumbizincicola* powder and 80 mL of deionized water were loaded in the vessel and sealed. The vessel was purged with nitrogen to remove residual air and heated up to pre-set temperature (i.e., 180°C , 220°C and 260°C). After desired reaction time (i.e., 0.5 h, 1 h, 2 h and 4 h), the vessel was cooled down to room temperature and the gaseous products were released. The remaining mixture was filtered through a $0.45\ \mu\text{m}$ PTFE membrane. The water-insoluble fraction was collected and extracted using acetone to separate acetone soluble and acetone-insoluble solid fractions. The acetone-insoluble solid was oven dried at 105°C and the obtained product was designated as hydrochar, which was labeled as HCX-Y, where HC stands for hydrochar, X indicates the temperature ($^\circ\text{C}$) and Y denotes the reaction time (h). Hydrochar yield was calculated using Eq. (1) and ash content was determined based on GB/T12496.3-1999.

$$\text{Hydrochar yield (\%)} = \frac{\text{dry weight of hydrochar}}{\text{dry weight of raw biomass}} \times 100\% \quad (1)$$

2.3. Physicochemical analysis of hydrochar adsorbents

Elemental compositions of raw biomass and hydrochars were analyzed using CHNS analyzer (Elementar vario EL, Germany). Surface functional groups of hydrochars before and after adsorption experiments were determined using Fourier transform infrared (FTIR) spectroscopy (Nicolet iS10, Thermo Fisher Scientific, USA). Proximate analysis was performed according to China National Standard (GB/T 28,731-2012). The acidity of raw biomass and hydrochars was determined using the method reported by Saha et al. (2019). The pH of point of zero charge (pH_{PZC}) of the materials was determined using an potentiometric mass titration method (Fiol and Villaescusa, 2009) using an automatic potentiometric titrator (Metrohm 905, Swiss). Zeta potential values were measured using Malvern zeta Sizer Nano series equipped with a rectangular electrophoresis cell. Improved Boehm titration method from Zhong et al. (2019) was used to quantitatively analyze the acidic oxygen functional groups on hydrochars. The surface area and pore size distributions of hydrochars were measured on Micromeritics Tristar II 3020 system using the Brunauer-Emmett-Teller (BET) and Barrett-Joyner-Halenda (BJH) methods. The morphology and elemental

Table 1
Physicochemical properties of *S. plumbizincicola*.

Ultimate analysis (wt.%)				Proximate analysis (wt.%)			HHV (MJ/kg)	Heavy metal concentration (mg/kg)						
C	H	N	O ^b	Ash	VM	FC		Cd	Cr	Pb	Zn	Fe	Mn	As
36.80	5.64	2.03	28.86	26.67	68.17	5.16	15.52	1222.63	134.19	371.54	35,165.50	7814.71	313.63	13.87

^a db, dry basis;

^b Calculated by difference.

HHV, higher heating value; VM, volatile matter; FC, fixed carbon.

distribution of hydrochars were analyzed using ZEISS Gemini 500.

2.4. Phosphate and ammonium adsorption experiment

2.4.1. Effect of solution pH

Hydrochars from HTC under different temperature for 2 h (i.e., HC180-2, HC220-2 and HC260-2) were selected for adsorption in a single solute system of phosphate and ammonium. Phosphate and ammonium stock solutions (1000 mg/L) were prepared to investigate the effect of initial solution pH (2–12) at 25 °C. Briefly, 0.1 g hydrochar and 100 mL phosphate or ammonium solution (100 mg/L) were loaded into a 250 mL beaker followed by shaking for 24 h (120 rpm) in a gas bath thermostat. After sorption experiment, samples were filtered through 0.22 μm membrane filter for analysis of residual concentration of phosphate and ammonium using ultraviolet spectrophotometry. All the experiments were performed in triplicate.

2.4.2. Effect of contact time and adsorption kinetics

Different contact times (0.5–40 h) were chosen to study the effect of contact time on the adsorption behavior at three different temperatures (25 °C, 35 °C and 45 °C). A constant adsorbent dosage of 1 g/L was used. The adsorption procedure was similar to that in Section 2.4.1. The data were then fitted with pseudo-first order equation (PFO, Eq. (2)) and pseudo-second order equation (PSO, Eq. (3)) to examine the adsorption kinetics.

$$q_t = q_e (1 - e^{-k_1 t}) \quad (2)$$

$$q_t = \frac{q_e^2 k_2 t}{1 + k_2 q_e t} \quad (3)$$

where q_e (mg/g) is the adsorption capacity at equilibrium, q_t (mg/g) is the adsorption capacity at any time t (min), k_1 (1/min) and k_2 (g/mg × min) are the rate constant of PFO and PSO, respectively.

2.4.3. Maximum adsorption capacity

Phosphate or ammonium solutions with different initial concentrations (10–400 mg/L for phosphate, 10–1000 mg/L for ammonium) were prepared. The experiments were conducted at different temperatures (25 °C, 35 °C and 45 °C) with identical adsorbent dosage (1 g/L) and contact time (24 h). The maximum adsorption capacity of adsorbents was calculated using Eq. (4).

$$q_e = \frac{(C_0 - C_e) \times m}{V} \quad (4)$$

where q_e (mg/g) is the adsorption capacity of adsorbents; C_0 and C_e (mg/L) are initial and equilibrium concentrations of phosphate or ammonium; V (L) is the volume of aqueous solution; m (g) is the mass of adsorbents.

The experimental data were fitted into non-linear form of Langmuir (Eq. (5)), Freundlich (Eq. (6)) isotherms.

$$Q_e = \frac{Q K_L C_e}{1 + K_L C_e} \quad (5)$$

$$Q_e = K_F C_e^{1/n} \quad (6)$$

where Q_e (mg/g) is the adsorption capacity and C_e (mg/L) is the equilibrium concentration in solution; Q (mg/g) is the maximum adsorption capacity of the adsorbent obtained from the Langmuir model; K_L (L/mg) is a constant related to the energy of adsorption; K_F (mg/g)/(mg/L)^{1/n} is the Freundlich constant; n (dimensionless) is the Freundlich intensity parameter.

2.4.4. Co-adsorption experiment

Effects of initial solution pH and concentration were examined during competitive adsorption of PO_4^{3-} and NH_4^+ . Specifically, 0.1 g HC260-

2 was applied in a 100 mL mixture of NH_4Cl and K_2HPO_4 with their initial concentration of 100 mg/L following the procedure in Section 2.4.1. Different initial P and N concentrations were employed. An initial concentration of 100 mg/L was constantly applied for PO_4^{3-} , while initial concentration of NH_4^+ was varied from 10 to 400 mg/L. For comparison, an initial NH_4^+ concentration of 100 mg/L was used with varied initial PO_4^{3-} concentration ranging from 10 to 400 mg/L.

3. Results and discussion

3.1. Characterization of hydrochars

3.1.1. Physicochemical properties

Table 2 summarizes physicochemical properties of raw biomass and hydrochars. The yield of hydrochar gradually decreased with the increase of reaction temperature and time. O/C and H/C atomic ratios were widely used to determine the polarity and aromaticity of biomass. H/C ratio generally decreased with increasing aromaticity (Xiao et al., 2016), which may indicate a higher stability (Zhao et al., 2019). The increased aromaticity of hydrochar at higher temperature in this study may facilitate its adsorption performance. Ash content in hydrochars generally increased with higher temperature and prolonged reaction time, and reached 56.41% for HC260-4, which may be due to the decomposition of water-soluble organic matter in hydrothermal reaction (Peterson et al., 2008). Besides, formation of metal oxides might also increase the ash content (Leng et al., 2018).

Raw biomass was slightly alkaline with pH of 7.4, but hydrochars showed a decreasing pH_{pzc} of after HTC under prolonged reaction time and increased temperature, suggesting increased acidity of hydrochars (Mathur and Moudgil, 1997). HC260-4 exhibited the lowest pH of 5.0, implying formation of acidic functional groups on the surface of hydrochar. SEM-EDS analysis further confirmed metallic compounds on the surface of hydrochar (Fig. S1) that could offer active sites for phosphate and ammonium adsorption through surface complexation or precipitation.

3.1.2. Acidic oxygen-containing functional groups

Adsorption capacity of hydrochar is affected by its acidic oxygen-containing functional groups on the surface which may act as the main adsorption sites (Zhang et al., 2019, 2020). In Table 3, total acidic oxygen-containing functional groups of hydrochars (630.8–1008.9 μmol/g) was higher than that of raw biomass (615 μmol/g) and achieved the maximum for HC260-4. Possible conversion of $-\text{COOH}$ into $-\text{C}=\text{O}$ in HTC at ca. 220 °C (He et al., 2013) and aromatization/polymerization on hydrochar surface (Saha et al., 2019) led to a slight increase of $-\text{COOH}$ but drastic increase of $-\text{C}=\text{O}$ in hydrochars, whereas the decreasing phenolic group was associated with hydrolysis (Saha et al., 2019). Decomposition of these functional groups may occur under severe HTC temperature (Reza et al., 2013), nevertheless, the ever increasing total acidic functional groups on hydrochars from this HTC below 260 °C could be favorable for adsorption capacity.

3.1.3. Textural characteristics

Textural characteristics, e.g., specific surface area (S_{BET}), pore size and volume, of raw biomass and hydrochars are presented in Table 3. S_{BET} of raw biomass was 1.746 m²/g which was much lower than that of hydrochars (3.241–25.115 m²/g). Pore volume and diameter tended to increase after mild hydrolysis below 220 °C but decreased with higher temperature to 260 °C and extended reaction time to 4 h, which may result from structure blockage by generated biocrude and tar (He et al., 2016). SEM images (Fig. S2) present a relatively smooth fibrous structure of raw biomass and ruptured fragments in hydrochars. Nevertheless, significantly smaller S_{BET} of hydrochar than biochar may indicate a more important role of oxygen-containing functional group on the surface of hydrochar in adsorption capacity rather than its textural properties (Masoumi et al., 2021; Wahab et al., 2010).

Table 2
Physicochemical properties of raw biomass and hydrochars.

Samples	Yield (%)	Elemental analysis (%)					O/C	H/C	Proximate analysis (%)			pH	pH _{pzc}
		C	H	N	O ^a	S			VM	FC	Ash		
Raw biomass	–	37.62	5.10	1.13	29.48	BD	0.78	0.14	68.17	5.16	26.67	7.42	5.95
HC180-0.5	65.12	37.94	5.56	1.22	30.16	BD	0.79	0.15	67.46	7.42	25.12	6.86	5.83
HC180-1	62.38	38.35	5.42	1.23	31.10	BD	0.81	0.14	65.42	10.68	23.90	6.34	5.75
HC180-2	59.64	38.05	5.33	1.25	30.41	BD	0.80	0.14	61.84	13.20	24.96	6.26	5.70
HC180-4	54.27	38.15	5.17	1.33	28.88	BD	0.76	0.14	60.49	13.04	26.47	5.94	5.45
HC220-0.5	50.82	35.47	4.70	1.13	30.54	BD	0.86	0.13	57.64	14.20	28.16	6.24	5.56
HC220-1	49.88	39.16	4.68	1.10	25.16	BD	0.64	0.12	56.43	13.67	29.90	5.86	5.22
HC220-2	48.06	36.65	4.65	1.18	25.10	BD	0.68	0.13	53.76	13.82	32.42	5.66	5.09
HC220-4	43.39	35.50	4.36	1.24	21.47	BD	0.60	0.12	51.94	10.63	37.43	5.53	4.92
HC260-0.5	45.73	30.03	3.50	1.20	15.60	BD	0.52	0.12	42.17	8.16	49.67	6.04	5.75
HC260-1	40.24	30.95	3.50	1.35	11.74	BD	0.38	0.11	41.07	6.47	52.46	5.76	5.43
HC260-2	37.35	28.39	3.24	1.21	13.54	BD	0.48	0.11	38.43	7.95	53.62	5.26	4.86
HC260-4	26.02	28.65	3.06	1.32	10.56	BD	0.37	0.11	37.46	6.13	56.41	5.03	4.73

^a Calculated by difference. BD, below detection limit. VM, volatile matter. FC, fixed carbon.

Table 3
Acidic oxygen-containing functional groups and textural properties of raw biomass and hydrochars.

Samples	Acidic oxygen-containing functional group (μmol/g dry mass)				Textural properties		
	Carboxylic (-COOH)	Lactone (-C=O)	Phenolic (-OH)	Total	S _{BET} (m ² /g)	V _{Total} (cm ³ /g)	D _a (nm)
Raw biomass	138.3 ± 3.2	54.9 ± 6.2	421.8 ± 9.4	615 ± 4.9	1.746	0.008	14.463
HC180-0.5	89.4 ± 2.6	50.1 ± 7.8	491.3 ± 4.7	630.8 ± 0.4	3.241	0.018	21.459
HC180-1	91.6 ± 8.4	67.5 ± 5.5	472.4 ± 8.4	631.5 ± 0.3	3.768	0.029	22.146
HC180-2	90.2 ± 11.2	89.1 ± 14.2	456.1 ± 9.0	635.4 ± 5.4	4.176	0.029	24.076
HC180-4	94.7 ± 1.8	132.4 ± 0.6	444.6 ± 1.5	671.7 ± 4.9	4.838	0.031	25.219
HC220-0.5	96.2 ± 2.7	178.0 ± 8.5	361.4 ± 1.7	635.6 ± 4.3	15.376	0.076	21.762
HC220-1	104.4 ± 2.1	188.3 ± 4.9	349.7 ± 4.2	642.4 ± 7.6	22.486	0.097	20.476
HC220-2	126.5 ± 6.4	207.6 ± 5.3	324.6 ± 4.4	658.7 ± 11.2	24.321	0.122	20.146
HC220-4	169.1 ± 5.3	251.4 ± 3.4	300.1 ± 1.9	720.6 ± 17.4	25.115	0.124	19.802
HC260-0.5	284.8 ± 4.2	342.6 ± 10.3	325.4 ± 4.6	952.8 ± 4.9	16.846	0.118	20.468
HC260-1	293.2 ± 4.9	351.0 ± 0.7	294.7 ± 3.7	938.9 ± 5.6	19.754	0.146	18.486
HC260-2	322.4 ± 2.8	366.7 ± 7.9	283.4 ± 2.8	972.5 ± 5.1	21.486	0.094	18.256
HC260-4	358.3 ± 3.0	381.2 ± 14.4	269.4 ± 6.7	1008.9 ± 13.4	20.542	0.089	17.380

3.2. Adsorption behaviors for phosphate and ammonium

3.2.1. Effect of initial solution pH

Increased pH from 2 to 12 led to a decreasing phosphate adsorption capacity from 40.68 to 10.86 mg/g (Fig. 1a). In aqueous solution, phosphate can exist in forms of H₃PO₄, H₂PO₄⁻, HPO₄²⁻, and PO₄³⁻ depending on the solution pH (Krishnan and Haridas, 2008), and pK_{a1}, pK_{a2}, and pK_{a3} of H₃PO₄ is 2.2, 7.2, 12.4, respectively. Therefore, the dominant species of phosphate were H₂PO₄⁻ and HPO₄²⁻ in this study. Under different solution pH, pH_{pzc} could significantly influence the adsorption behavior. For instance, adsorbent exhibits a positive surface

charge when the solution pH is lower than pH_{pzc}, vice versa. The pH_{pzc} of hydrochar was in the range of 4.73–5.83 (Table 2 and Fig. S3). In acidic solution, the negatively charged phosphate species would be adsorbed by the positively charged hydrochar. However, with the increased pH under alkaline condition, the electrostatic repulsion between phosphate species and negatively charged adsorbent will be enhanced, resulting in a decrease in phosphate adsorption capacity. Moreover, at higher pH, the competition between hydroxide ions and negatively charged phosphate species on the adsorbent surface could also inhibit the adsorption capacity (Lalley et al., 2016; Lu et al., 2013). The pH value increased after phosphate adsorption in the experiment with an initial pH of 2–6

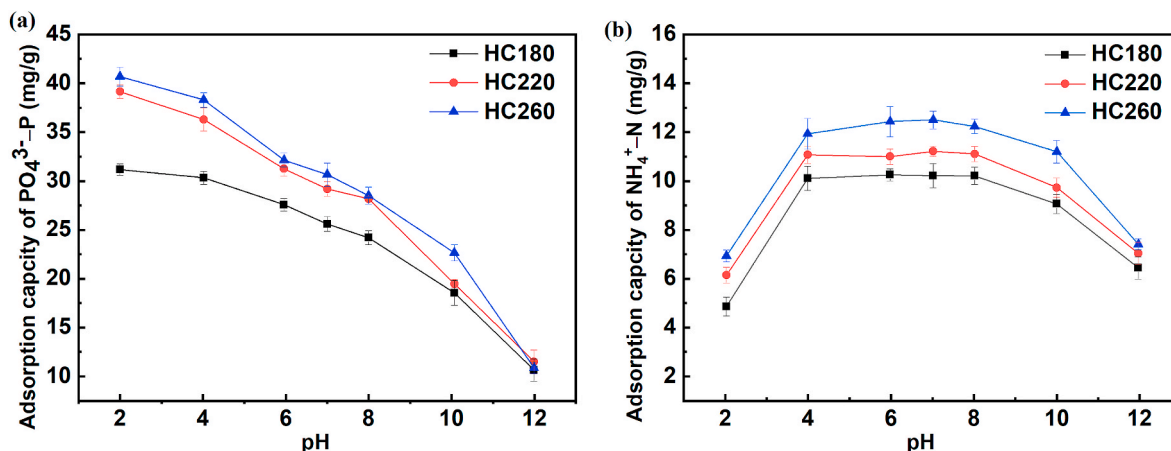


Fig. 1. Effect of pH on (a) phosphate and (b) ammonium adsorption.

(Fig. S4a), which could be attributed to the protonation of oxygen-containing functional groups. When the initial pH was between 6 and 10, the pH after adsorption slightly increased, which was probably related to the replacement of hydroxyl on the surface of the metal oxides by PO_4^{3-} , and the released hydroxyl resulted in an increased pH. When initial pH was 10–12, the pH after adsorption remained stable because the decreased PO_4^{3-} adsorption capacity inhibited the replacement of hydroxyl on the surface of metal oxides. The pH_{pzc} dropped to 3.36 after phosphate adsorption (Fig. S3), indicating an increase of negative ions on the surface of hydrochar after the adsorption process (Bowden et al., 1980).

With the increase of pH from 2 to 4, the NH_4^+ adsorption capacity was dramatically increased and became stable in an optimal pH range of 4–8 (Fig. 1b). Further increased pH caused a noticeable decrease of this adsorption capacity. Nitrogen could exist in forms of NH_4^+ and NH_3 in aqueous solution (Clément and Merlin, 1995). NH_4^+ is predominate in acidic and neutral solution (Al-Ghouti et al., 2019). The surface of hydrochar was positively charged when the solution pH was lower than pH_{pzc} (4.23) (Fig. S3), thereby repelling NH_4^+ . Moreover, there was also competition between free hydrogen ion (H^+) and cationic NH_4^+ at lower pH. Thus, ion exchange may be the main mechanism for NH_4^+ adsorption. The negatively charged hydrochar became under increasing pH was beneficial to NH_4^+ adsorption. However, at high pH above 10, the majority of NH_4^+ will be transformed into NH_3 that cannot be effectively adsorbed by hydrochar. Because of the surface protonation, the equilibrium pH after NH_4^+ adsorption was slightly higher than that of original pH when the initial pH was in the range of 2–5. But it became lower when initial pH was higher than 7 was applied in adsorption (Fig. S4b) as a consequence of consumed OH^- in the formation of NH_3 . Accordingly, the pH_{pzc} was increased to 5.14 after NH_4^+ adsorption.

3.2.2. Adsorption kinetics

As depicted in Figs. 2 and 3, under a higher adsorption temperature of 45 °C, adsorption capacity of three hydrochars for PO_4^{3-} (37.65–49.15 mg/g) and NH_4^+ (15.18–17.60 mg/g) was more favored with HC260 exhibiting the highest adsorption performance. The adsorption achieved equilibrium after 8 h.

Adsorption kinetics was studied with two different kinetic models to obtain corresponding parameters (Tables S1 and S2). The equilibrium adsorption capacity (q_e) obtained from PFO and PSO model was close to the experimental data. The PFO model is usually used to describe the diffusional kinetics, while the PSO model generally reveals the mechanism of adsorption related to active sites of the adsorbent (Wang and Guo, 2020). Regarding phosphate adsorption, both PFO and PSO model provided good fit to the experimental data ($R^2 > 0.98$), suggesting that both internal diffusion and chemisorption played an important role in the adsorption process. However, the PSO model gave a better fit to the experimental data for ammonium adsorption, indicating that the functional groups on the surface of hydrochar acted as binding sites for the removal of ammonium from the aqueous solution (Wang and Guo,

2020). Higher k values in these two models revealed that higher temperature facilitated the adsorption rate.

3.2.3. Adsorption isotherms

Adsorption capacity of hydrochar for PO_4^{3-} and NH_4^+ was improved by increasing initial concentration and adsorption temperature. Maximum adsorption capacity for PO_4^{3-} (52.46 mg/g) and NH_4^+ (27.56 mg/g) was obtained on HC260-2 at 45 °C, but slightly decreased to 48.36 mg/g and 21.53 mg/g, respectively, at 25 °C (Figs. S5 and S6). After experimental data fitting using the non-linear Langmuir and Freundlich models, parameters from the models are derived and summarized in Tables 4 and 5. Langmuir model gave a better fit with higher R^2 values for adsorption of PO_4^{3-} and NH_4^+ . Generally, the Langmuir assumes monolayer adsorption onto a surface containing a fixed number of accessible active sites with no interactions among adsorbate species and no further adsorption can occur when a site was occupied (Desta, 2013; Tran et al., 2017).

3.2.4. Evolution of surface functional groups on hydrochar

Fig. 4 describes the FTIR spectra of hydrochars before and after adsorption of PO_4^{3-} and NH_4^+ . The band at $\sim 3400 \text{ cm}^{-1}$ was due to the stretching vibration of O–H from hydroxyl group (Fleming and Williams, 2019), while peaks at 2920 and 2850 cm^{-1} were ascribed to asymmetric and symmetric stretching of C–H (de Oliveira Silva et al., 2012). Bands at 1615 and 1010 cm^{-1} represented the stretching vibration of C=O and C–O, respectively (Li et al., 2011). After the adsorption, the O–H peak became less intense, suggesting that hydroxyl or carboxyl groups had reacted with phosphate or ammonium through hydrogen bonding and/or complexation (Wu et al., 2020). In addition, a new peak at 1093 cm^{-1} appeared after phosphate adsorption, which was assigned to the symmetric stretching of P–O bond (Stoch et al., 2016). This confirmed that PO_4^{3-} was successfully adsorbed onto hydrochar.

3.3. Co-adsorption of PO_4^{3-} and NH_4^+ on hydrochar

Efficient adsorption of PO_4^{3-} and NH_4^+ onto as-prepared hydrochar was observed in a single solute adsorption. Nevertheless, nitrogen and phosphorous rarely exist alone in practical application, especially in the eutrophic water bodies. Therefore, it is important to explore the competitive interaction of PO_4^{3-} and NH_4^+ onto the hydrochar in aqueous solution.

3.3.1. Effect of solution pH

Fig. 5 presents the influence of solution pH on the co-adsorption of PO_4^{3-} and NH_4^+ . The competitive adsorption system slightly enhanced the NH_4^+ adsorption onto the hydrochar under the same solution pH, whereas the adsorption of PO_4^{3-} was not obviously affected. In the single solute adsorption system, the highest NH_4^+ adsorption capacity of HC260-2 was 12.76 mg/g at pH 7 that increased to 17.55 mg/g at pH 6 in the co-adsorption system. The enhanced adsorption capacity was

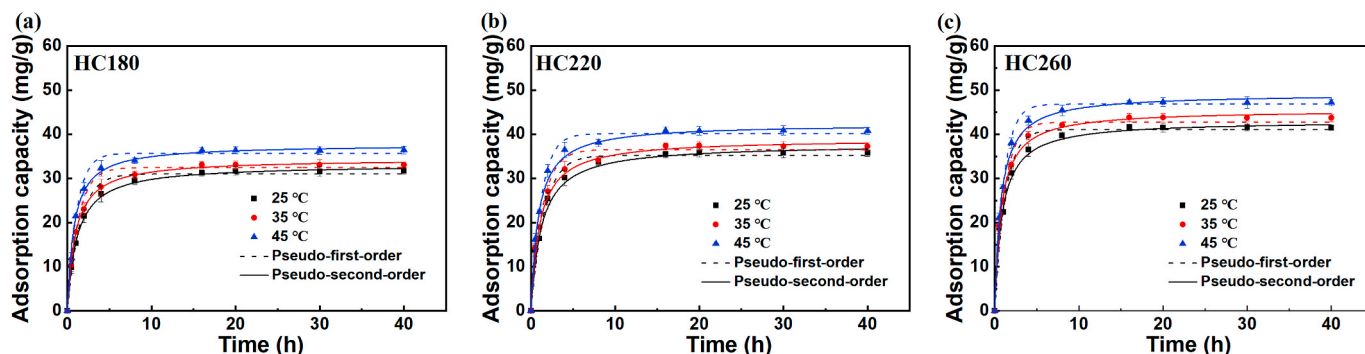


Fig. 2. Phosphate adsorption kinetics by hydrochars.

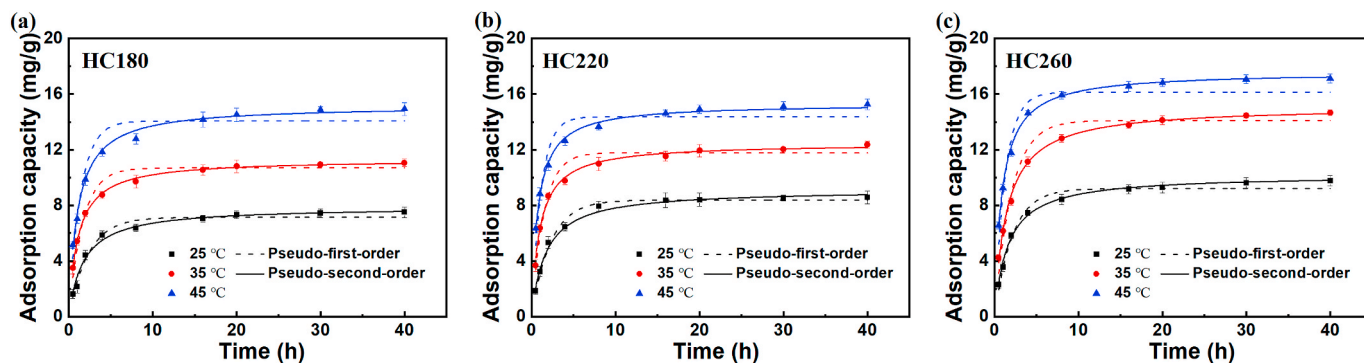


Fig. 3. Ammonium adsorption kinetics by hydrochars.

Table 4
Parameters of adsorption isotherms for phosphate under different temperatures.

Temperature (°C)	Sorbent	Langmuir model			Freundlich model		
		K_L (L/mg)	Q (mg/g)	R^2	K_F (mg/g)/(mg/L) ^{1/n}	1/n	R^2
25	HC180	0.0408	39.1459	0.9689	7.1318	0.2922	0.7971
	HC220	0.0374	45.5298	0.9848	7.4784	0.3105	0.8453
	HC260	0.0346	54.4109	0.9732	8.2597	0.3233	0.8282
35	HC180	0.0582	42.2846	0.9631	7.6392	0.2913	0.8320
	HC220	0.0623	47.7898	0.9732	11.1940	0.2559	0.9013
	HC260	0.0767	53.5539	0.9736	13.9212	0.2341	0.8659
45	HC180	0.0988	42.8463	0.9923	12.4474	0.2205	0.8962
	HC220	0.0922	48.5625	0.9828	10.6371	0.2297	0.8925
	HC260	0.1029	53.5995	0.9766	15.7468	0.2245	0.8766

Table 5
Parameters of adsorption isotherms for ammonium under different temperatures.

Temperature (°C)	Sorbent	Langmuir model			Freundlich model		
		K_L (L/mg)	Q (mg/g)	R^2	K_F (mg/g)/(mg/L) ^{1/n}	1/n	R^2
25	HC180	0.0163	16.9534	0.9933	2.0665	0.3070	0.8588
	HC220	0.0200	20.1078	0.9949	1.3738	0.3909	0.9337
	HC260	0.0220	21.6211	0.9905	1.8392	0.3615	0.9353
35	HC180	0.0222	23.4338	0.9852	2.2483	0.3402	0.8756
	HC220	0.0247	24.6372	0.9919	2.0345	0.3706	0.8680
	HC260	0.0256	25.0599	0.9926	4.9742	0.2437	0.7332
45	HC180	0.0254	23.9359	0.9815	3.3298	0.2844	0.7876
	HC220	0.0257	24.9512	0.9904	3.2648	0.3021	0.8281
	HC260	0.0283	27.2951	0.9914	5.1959	0.2482	0.8195

more obvious especially under weak acid solution. The presence of anionic PO_4^{3-} probably established an effective electrostatic shielding against the repulsion force of cationic NH_4^+ in the adjacent sites, thereby promoting NH_4^+ adsorption (Navarro et al., 2001). The H^+ ions under acidic solution would compete for the adsorption sites of NH_4^+ (Yin et al., 2019), while the negatively charged hydrochar ($\text{pH} > \text{pH}_{\text{pzc}}$) under increased pH favored NH_4^+ adsorption. On the other hand, the effect of pH on the adsorption of phosphate onto the hydrochar was not noticeable as compared to that in single solute system, which may be attributed to higher selective adsorption of PO_4^{3-} than NH_4^+ .

3.3.2. Effect of initial solute concentration

Fig. 6 demonstrates the competitive adsorption of PO_4^{3-} and NH_4^+ under various initial solute concentration ratios of $\text{PO}_4^{3-}:\text{NH}_4^+$. NH_4^+ adsorption was enhanced when initial concentration of PO_4^{3-} was below 100 mg/L but decreased under higher PO_4^{3-} above 100 mg/L. Char-based materials preferentially reacted with PO_4^{3-} via stronger chemical bonds, whereas the reaction with NH_4^+ was mainly via hydrogen bonds (Yin et al., 2019). Thus, stronger chemical bonds between hydrochar and PO_4^{3-} under higher PO_4^{3-} concentration resulted in a decreased NH_4^+ adsorption. Moreover, abundant metal ions on the hydrochar surface, e.

g., Zn^{2+} , $\text{Fe}^{2+/3+}$, Cd^{2+} could react with PO_4^{3-} under higher concentration (Inglezakis, 2005), which further reduced the amount of bonding sites for NH_4^+ adsorption. Regarding PO_4^{3-} adsorption, lower NH_4^+ concentration (10–50 mg/L) promoted PO_4^{3-} adsorption, however, the adsorption capacity slightly decreased when initial PO_4^{3-} concentration was increased from 100 to 400 mg/L. The complexation of NH_4^+ with metal oxide on hydrochar surface could stabilize phosphate species therein (Huang et al., 2010; Liu et al., 2016). Besides, electrostatic shielding may also occur when NH_4^+ was present in lower concentration. Nevertheless, excess ammonium ions in the solution could occupy most of the available active sites and hinder the adsorption capacity towards PO_4^{3-} . In addition, K^+ was also introduced into the system via K_2HPO_4 in this study. Guaya et al. (2016) found that the presence of K^+ in solution significantly reduced adsorption capacity of ammonium onto zeolite. Hence, in this co-adsorption system, synergistic and competitive reaction may occur simultaneously, and the adsorption behavior can be affected by various factors.

3.4. Adsorption mechanism

In general, mechanism for PO_4^{3-} and NH_4^+ adsorption onto

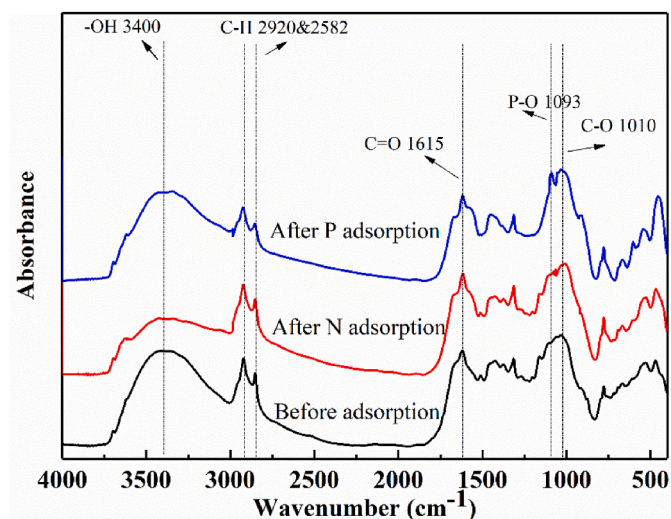


Fig. 4. FTIR spectra of hydrochars before and after adsorption of PO_4^{3-} and NH_4^+ .

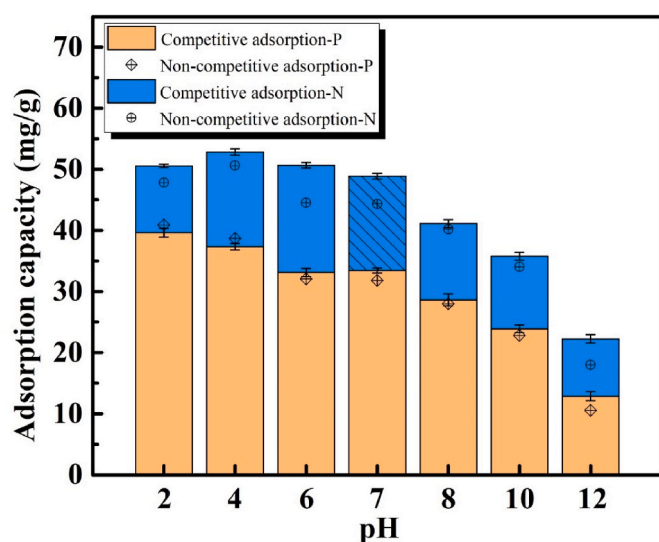


Fig. 5. Co-adsorption of phosphate and ammonium under different solution pH values.

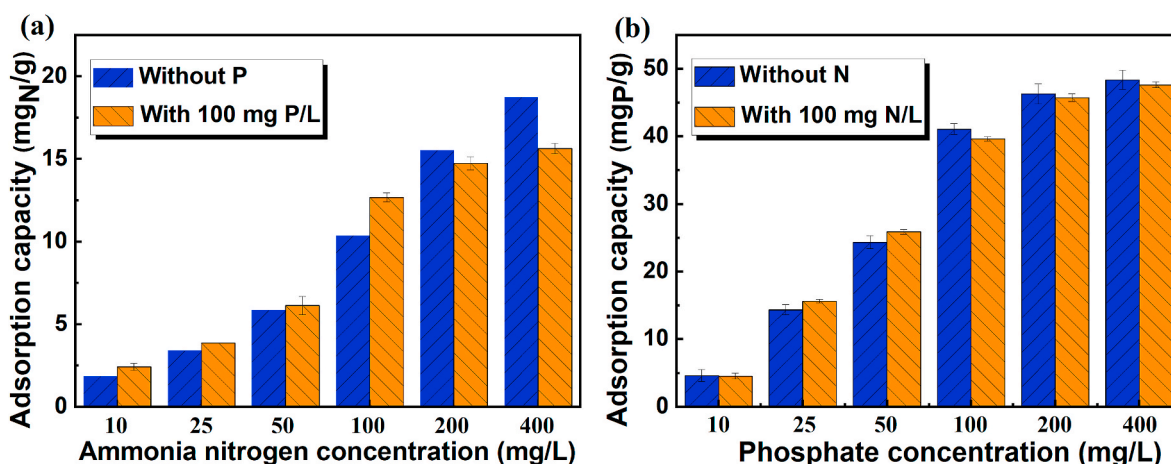


Fig. 6. Competitive adsorption of phosphate and ammonium.

hydrochars mainly involves electrostatic attraction, complexation, physical adsorption and chemical precipitation. Kinetics studies indicated that chemisorption played an important role in the adsorption process, and internal diffusion was also significant in PO_4^{3-} adsorption. Although increasing HTC temperature from 220 to 260 $^{\circ}\text{C}$ resulted in a decrease in specific surface area, pore volume and diameter of hydrochars, adsorption capacity of hydrochar towards PO_4^{3-} and NH_4^+ was enhanced. This implies that surface functional groups could be responsible for the adsorption process. The pH_{pzc} of hydrochar can be also affected by surface functional groups, thereby significantly affecting the adsorption behavior via electronic attraction. In addition, the naturally bonded metal cations on hydrochar surface may also improve its adsorption capacity for PO_4^{3-} and NH_4^+ through chemical precipitation.

4. Conclusions

S. plumbizincicola has been successfully fabricated into superior hydrochar adsorbent for effective nutrients recovery. Due to improved surface functional groups, the obtained hydrochar demonstrated good adsorption capacity towards PO_4^{3-} and NH_4^+ . The adsorption process was dominated by complexation with surface functional groups, electrostatic attraction and chemical precipitation on hydrochar. In co-adsorption, NH_4^+ adsorption was improved but PO_4^{3-} was not obviously affected. Synergistic co-adsorption of PO_4^{3-} and NH_4^+ occurred at lower concentrations, which could be attributed to the electrostatic shielding and the stabilization of PO_4^{3-} in the presence of NH_4^+ through complexation with metal oxides. The nutrients-enriched hydrochar would be applied as *in-situ* fertilizer for phytoremediation of contaminated sites with minimized environmental risks to close the loop.

Credit author statement

Ruichi Zhang: Investigation, Data Curation, Writing - Original Draft. **Yizhong Zhang:** Investigation, Writing - Review & Editing. **Ronn Goei:** Writing - Review & Editing. **Wen-Da Oh:** Writing - Review & Editing. **Zhao Zhang:** Investigation, Data Curation. **Chao He:** Conceptualization, Writing - Review & Editing, Supervision, Project administration, Funding acquisition.

Declaration of competing interest

The authors declare that they have no known competing financial interests or personal relationships that could have appeared to influence the work reported in this paper.

Data availability

Data will be made available on request.

Acknowledgement

C.H. acknowledges the Academy Research Fellowship and its research project funded by Research Council of Finland (decision numbers: 341052, 346578), and the starting grant from Tampere University. Y.Z. thanks the financial support from the Basic Research Funds of the Central Public Welfare Research Institute (Nos. R-JBYWF-2021-D04, K-JBYWF-2021-ZT04, and R-JBYWF-2021-D05).

Appendix B. Supplementary data

Supplementary data to this article can be found online at <https://doi.org/10.1016/j.jenvman.2023.118441>.

References

- Al-Ghouti, M.A., Al-Kaabi, M.A., Ashfaq, M.Y., Da'na, D.A., 2019. Produced water characteristics, treatment and reuse: a review. *J. Water Process Eng.* 28, 222–239.
- Bowden, J., Nagarajah, S., Barrow, N., Posner, A., Quirk, J., 1980. Describing the adsorption of phosphate, citrate and selenite on a variable-charge mineral surface. *Soil Res.* 18 (1), 49–60.
- Clément, B., Merlin, G., 1995. The contribution of ammonia and alkalinity to landfill leachate toxicity to duckweed. *Sci. Total Environ.* 170 (1), 71–79.
- Cui, X., Li, X., Zhang, J., Lin, Q., Xiao, H., Cheng, Z., Yan, B., Yang, X., Chen, G., 2022. Hydrothermal treatment of the pristine and contaminated Cd/Zn hyperaccumulators for bio-oil production and heavy metal separation. *ACS Sustain. Chem. Eng.* 10 (1), 603–612.
- Cui, X., Zhang, J., Wang, X., Pan, M., Lin, Q., Khan, K.Y., Yan, B., Li, T., He, Z., Yang, X., Chen, G., 2021. A review on the thermal treatment of heavy metal hyperaccumulator: fates of heavy metals and generation of products. *J. Hazard Mater.* 405, 123832.
- de Oliveira Silva, J., Filho, G.R., da Silva Meireles, C., Ribeiro, S.D., Vieira, J.G., da Silva, C.V., Cerqueira, D.A., 2012. Thermal analysis and FTIR studies of sewage sludge produced in treatment plants. The case of sludge in the city of Uberlândia-MG, Brazil. *Thermochim. Acta* 528, 72–75.
- Desta, M.B., 2013. Batch sorption experiments: Langmuir and Freundlich isotherm studies for the adsorption of textile metal ions onto teff straw (*Eragrostis tef*) agricultural waste. *J. Thermodynamics*, 375830, 2013.
- Fiol, N., Villaescusa, I., 2009. Determination of sorption point zero charge: usefulness in sorption studies. *Environ. Chem. Lett.* 7 (1), 79–84.
- Fleming, I., Williams, D., 2019. Infrared and Raman spectra. In: Fleming, I., Williams, D. (Eds.), *Spectroscopic Methods in Organic Chemistry*. Springer International Publishing, Cham, pp. 85–121.
- Francis-Floyd, R., Watson, C., Petty, D., Poudel, D.B., 2009. Ammonia in Aquatic Systems, vol. 16. UF/IFAS University of Florida (UF)/Institute of Food and Agricultural Sciences (IFAS), FA, pp. 1–4.
- Guaya, D., Valderrama, C., Farran, A., Cortina, J.L., 2016. Modification of a natural zeolite with Fe(III) for simultaneous phosphate and ammonium removal from aqueous solutions. *J. Chem. Technol. Biotechnol.* 91 (6), 1737–1746.
- He, C., Giannis, A., Wang, J.-Y., 2013. Conversion of sewage sludge to clean solid fuel using hydrothermal carbonization: hydrochar fuel characteristics and combustion behavior. *Appl. Energy* 111, 257–266.
- He, C., Zhao, J., Yang, Y., Wang, J.-Y., 2016. Multiscale characteristics dynamics of hydrochar from hydrothermal conversion of sewage sludge under sub- and near-critical water. *Bioresour. Technol.* 211, 486–493.
- Huang, H., Xiao, X., Yan, B., Yang, L., 2010. Ammonium removal from aqueous solutions by using natural Chinese (Chende) zeolite as adsorbent. *J. Hazard Mater.* 175 (1), 247–252.
- Inglezakis, V.J., 2005. The concept of “capacity” in zeolite ion-exchange systems. *J. Colloid Interface Sci.* 281 (1), 68–79.
- Jin, H., Yan, D., Zhu, N., Zhang, S., Zheng, M., 2019. Immobilization of metal(loid)s in hydrochars produced from digested swine and dairy manures. *Waste Manag.* 88, 10–20.
- Krishnan, K.A., Haridas, A., 2008. Removal of phosphate from aqueous solutions and sewage using natural and surface modified coir pith. *J. Hazard Mater.* 152 (2), 527–535.
- Lalley, J., Han, C., Li, X., Dionysiou, D.D., Nadagouda, M.N., 2016. Phosphate adsorption using modified iron oxide-based sorbents in lake water: kinetics, equilibrium, and column tests. *Chem. Eng. J.* 284, 1386–1396.
- Leng, L., Leng, S., Chen, J., Yuan, X., Li, J., Li, K., Wang, Y., Zhou, W., 2018. The migration and transformation behavior of heavy metals during co-liquefaction of municipal sewage sludge and lignocellulosic biomass. *Bioresour. Technol.* 259, 156–163.
- Li, M., Li, W., Liu, S., 2011. Hydrothermal synthesis, characterization, and KOH activation of carbon spheres from glucose. *Carbohydr. Res.* 346 (8), 999–1004.
- Li, Z., Wu, L., Hu, P., Luo, Y., Zhang, H., Christie, P., 2014. Repeated phytoextraction of four metal-contaminated soils using the cadmium/zinc hyperaccumulator *Sedum plumbizincicola*. *Environ. Pollut.* 189, 176–183.
- Liao, X., Chen, T., Xie, H., Xiao, X., 2004. Effect of application of P fertilizer on efficiency of As removal from As-contaminated soil using phytoremediation: field study. *Acta Sci. Circumstantiae* 24 (3), 455–462.
- Liu, T., Chang, B., Wu, K., 2016. The performance of phosphate removal using aluminium-manganese bimetal oxide coated zeolite: batch and dynamic adsorption studies. *Desalination Water Treat.* 57 (9), 4220–4233.
- Lü, J., Liu, H., Liu, R., Zhao, X., Sun, L., Qu, J., 2013. Adsorptive removal of phosphate by a nanostructured Fe–Al–Mn trimetal oxide adsorbent. *Powder Technol.* 233, 146–154.
- Ma, Y., Rajkumar, M., Luo, Y., Freitas, H., 2013. Phytoextraction of heavy metal polluted soils using *Sedum plumbizincicola* inoculated with metal mobilizing *Phyllobacterium myrsinacearum* RC6b. *Chemosphere* 93 (7), 1386–1392.
- Masoumi, S., Borugadda, V.B., Nanda, S., Dalai, A.K., 2021. Hydrochar: a review on its production technologies and applications. *Catalysts* 11 (8), 939.
- Mathur, S., Moudgil, B.M., 1997. Adsorption mechanism(s) of poly(ethylene oxide) on oxide surfaces. *J. Colloid Interface Sci.* 196 (1), 92–98.
- Navarro, R.R., Tatsumi, K., Sumi, K., Matsumura, M., 2001. Role of anions on heavy metal sorption of a cellulose modified with poly(glycidyl methacrylate) and polyethyleneimine. *Water Res.* 35 (11), 2724–2730.
- Peterson, A.A., Vogel, F., Lachance, R.P., Fröling, M., Antal, J.M.J., Tester, J.W., 2008. Thermochemical biofuel production in hydrothermal media: a review of sub- and supercritical water technologies. *Energy Environ. Sci.* 1 (1), 32–65.
- Pivetz, B.E., 2001. Phytoremediation of Contaminated Soil and Ground Water at Hazardous Waste Sites. US Environmental Protection Agency, Office of Research and Development.
- Reza, M.T., Yan, W., Uddin, M.H., Lynam, J.G., Hoekman, S.K., Coronella, C.J., Vásquez, V.R., 2013. Reaction kinetics of hydrothermal carbonization of loblolly pine. *Bioresour. Technol.* 139, 161–169.
- Saha, N., Saba, A., Reza, M.T., 2019. Effect of hydrothermal carbonization temperature on pH, dissociation constants, and acidic functional groups on hydrochar from cellulose and wood. *J. Anal. Appl. Pyroly.* 137, 138–145.
- Stoch, P., Stoch, A., Ciecinska, M., Krakowiak, I., Sitarz, M., 2016. Structure of phosphate and iron-phosphate glasses by DFT calculations and FTIR/Raman spectroscopy. *J. Non-Cryst. Solids* 450, 48–60.
- Tan, X.-f., Liu, S.-b., Liu, Y.-g., Gu, Y.-l., Zeng, G.-m., Hu, X.-j., Wang, X., Liu, S.-h., Jiang, L.-h., 2017. Biochar as potential sustainable precursors for activated carbon production: multiple applications in environmental protection and energy storage. *Bioresour. Technol.* 227, 359–372.
- Tran, H.N., You, S.-J., Hosseini-Bandegharaei, A., Chao, H.-P., 2017. Mistakes and inconsistencies regarding adsorption of contaminants from aqueous solutions: a critical review. *Water Res.* 120, 88–116.
- Vikrant, K., Kim, K.-H., Ok, Y.S., Tsang, D.C.W., Tsang, Y.F., Giri, B.S., Singh, R.S., 2018. Engineered/designer biochar for the removal of phosphate in water and wastewater. *Sci. Total Environ.* 616–617, 1242–1260.
- Wahab, M.A., Jellali, S., Jedidi, N., 2010. Ammonium biosorption onto sawdust: FTIR analysis, kinetics and adsorption isotherms modeling. *Bioresour. Technol.* 101 (14), 5070–5075.
- Wang, J., Guo, X., 2020. Adsorption kinetic models: physical meanings, applications, and solving methods. *J. Hazard Mater.* 390, 122156.
- Wu, B., Wan, J., Zhang, Y., Pan, B., Lo, I.M.C., 2020. Selective phosphate removal from water and wastewater using sorption: process fundamentals and removal mechanisms. *Environ. Sci. Technol.* 54 (1), 50–66.
- Xiao, X., Chen, Z., Chen, B., 2016. H/C atomic ratio as a smart linkage between pyrolytic temperatures, aromatic clusters and sorption properties of biochars derived from diverse precursors. *Sci. Rep.* 6 (1), 22644.
- Yin, Q., Liu, M., Ren, H., 2019. Biochar produced from the co-pyrolysis of sewage sludge and walnut shell for ammonium and phosphate adsorption from water. *J. Environ. Manag.* 249, 109410.
- Zhang, T., Wu, X., Fan, X., Tsang, D.C.W., Li, G., Shen, Y., 2019. Corn waste valorization to generate activated hydrochar to recover ammonium nitrogen from compost leachate by hydrothermal assisted pretreatment. *J. Environ. Manag.* 236, 108–117.
- Zhang, T., Wu, X., Shaheen, S.M., Zhao, Q., Liu, X., Rinklebe, J., Ren, H., 2020. Ammonium nitrogen recovery from digestate by hydrothermal pretreatment followed by activated hydrochar sorption. *Chem. Eng. J.* 379, 122254.
- Zhao, Z., Nie, T., Zhou, W., 2019. Enhanced biochar stabilities and adsorption properties for tetracycline by synthesizing silica-composited biochar. *Environ. Pollut.* 254, 113015.
- Zhong, D., Jiang, Y., Zhao, Z., Wang, L., Chen, J., Ren, S., Liu, Z., Zhang, Y., Tsang, D.C.W., Crittenden, J.C., 2019. pH dependence of arsenic oxidation by rice-husk-derived biochar: roles of redox-active moieties. *Environ. Sci. Technol.* 53 (15), 9034–9044.
- Zhou, J., Shao, L., Zhu, H., Wei, Z., Wu, Q., 2014. Phytoremediation of inter-cropping with chemical enhancement of heavy-metal-contaminated acid soil: a long-term field experiment. *Acta Pedol. Sin.* 51 (5), 1056–1065.